Design and Synthesis of Highly Active Al–Ni–P Foam Electrode for Hydrogen Evolution Reaction

ARTICLE *in* ACS CATALYSIS · SEPTEMBER 2015

Impact Factor: 9.31 · DOI: 10.1021/acscatal.5b01761

ACS Catalysis

Letter

pubs.acs.org/acscatalysis

Design and Synthesis of Highly Active Al−Ni−P Foam Electrode for Hydrogen Evolution Reaction

José Luis Lado,[†] Xiaoguang Wang,[†] Elvira Paz,[†] Enrique Carbó-Argibay,[†] Noelia Guldris,[†] Carlos Rodríguez-Abreu,[†] Lifeng Liu,[†] Kirill Kovnir,[‡] and Yury V. Kolen'ko*[,†]

[†]International Iberian Nanotechnology Laboratory, Braga 4715-330, Portugal

[‡]Department of Chemistry, University of California, Davis, Davis, California 95616, United States

Supporting Information

ABSTRACT: An effective method to boost the electrocatalytic activity of nickel phosphides in H_2 evolution reaction is reported. The method took advantage of density functional theory calculations that allowed the design of a highly active material based on the combination of d-metal with p-metal within a phosphide structure. Furthermore, the principle is proven experimentally through successful synthesis of self-supported ternary Al−Ni−P foam electrocatalyst by alloying of Ni and Al followed by the gas transport phosphorization reaction. As a cathode for H_2 evolution reaction in acidic electrolyte, Al−Ni−P significantly outperforms pure Ni−P, and it has an exchange current density of 0.6 mA/cm^2 and a Tafel slope of 65 mV/decade.

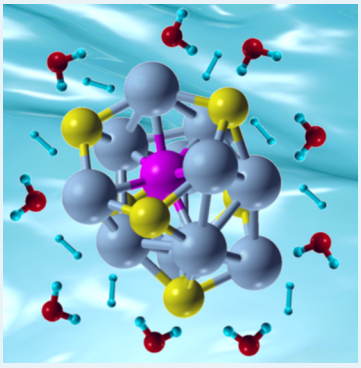

KEYWORDS: *DFT, ELF, electrocatalysis, hydrogen evolution reaction, nickel phosphide, doping, Tafel slope*

The hydrogen evolution reaction (HER) is the cathodic half reaction of electrochemical water splitting, $2H^+ + 2e^- \rightarrow H_2\uparrow$, which plays a crucial role in the generation of environmentally friendly H_2 fuels. This process is typically conducted in highly alkaline or highly acidic conditions, and it occurs through two consecutive steps, namely, the dissociation reaction (Volmer step) followed by the H_2 evolving via parallel and competitive chemical (Tafel step) or electrochemical (Heyrovsky step) desorptions.[1−3]

Currently, the most efficient electrodes for HER contain precious Pt, which is a benchmark electrocatalyst for HER process showing exchange current density, i_0, of about 1 mA/cm^2 and a Tafel slope of 30 mV/decade.[4] Limited availability and high price of Pt have sparked extensive research efforts toward the search for novel high-performing HER electrocatalysts that use only earth-abundant elements. At present, the most active and cost-effective materials include transition-metal alloys, sulfides, carbides, and phosphides.[3,5,6]

Among the aforementioned materials, nickel phosphide with tailored particle size, morphology, and phase composition is the most prominent material,[5] offering high activity and reduced corrosiveness in HER.[7,8] In this context, we have recently developed convenient phosphorization methods of commercially available Ni foam that resulted in efficient self-supported Ni−P nanorods or nanosheet array cathodes exhibiting remarkable activity and durability in HER.[9,10] Despite these successes, Pt-based electrocatalysts have not been outperformed, and the examples of highly active and stable Pt-free electrocatalysts are still scarce.

Hydrogenation catalysts are also known to show good performance in HER because both processes are determined by the adsorption of intermediate H atoms.[3] In hydrogenation, efficient alternatives to the classical noble metal catalysts are offered by 3d transition-metal alloys and intermetallic compounds.[11,12] In most cases, high activity of the alloy catalysts is explained by a combination of geometrical effects, such as the active-site isolation concept,[13] and electronic effects, due to chemical bonding perturbation.[14,15] To improve the activity of Ni−P cathodes for HER, we hypothesized that alloying of Ni d-metal with Al p-metal followed by phosphorization would produce a new class of abundant and highly efficient ternary Al−Ni−P electrocatalysts for HER. Surprisingly, thus far, no ternary Al−Ni−P bulk compounds have been synthesized and structurally characterized. A possible disadvantage of Al-containing HER catalysts may be leaching of Al in acidic or alkaline solution. Ni_3Al intermetallic cathode has, however, shown good corrosion resistance during HER.[16] Additionally, slow dissolution of Al during HER can be beneficial to increase the surface area of Ni−P electrocatalysts in a process resembling the formation of Raney Ni.[17]

In general, Al atoms are not expected to serve as active sites, but Al rather acts as a dopant to influence the electronic structure of Al−Ni−P and surface adsorption energy of the reactants.[12,13,18] Using density functional theory (DFT), we

Received: August 12, 2015
Revised: September 23, 2015

DOI: 10.1021/acscatal.5b01761
ACS Catal. 2015, 5, 6503−6508

found that Al doping modifies the density of states of nickel phosphides by developing and broadening of overall band structure and introducing significant covalent bonding component, while preserving the metallic nature. Herein, we synthesize a novel and highly active ternary Al−Ni−P electrocatalyst, demonstrating the potential of an Al p-metal alloying strategy for enhancing the performance of binary Ni−P electrocatalysts.

To understand the crystal and electronic structure of the hypothesized novel class of electrocatalysts based on the combination of p- and d-metals, we undertook DFT analysis of various Al-doped Ni−P systems using the Elk (FP-LAPW) and Quantum Espresso (pseudopotential) codes.[19,20] The synthesized self-supported Ni−P cathode is a mixture of two nickel phosphides, Ni_5P_4 and Ni_2P.[9,10] Therefore, both compounds were scrutinized by theory on the changes of the electronic structure as a function of Al incorporation (Figure 1). The main

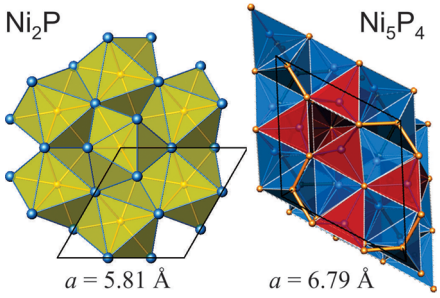

Figure 1. Polyhedral representation of the crystal structures of Ni_2P (left) and Ni_5P_4 (right) viewed along [001] direction. Unit cells are shown with black lines. Ni: blue; P: yellow.

structural unit in Ni_2P consists of $P@Ni_9$ tricapped trigonal prisms (yellow polyhedra in Figure 1, left), which are condensed into a 3D framework by sharing the faces. In turn, in Ni_5P_4, the homoatomic P−P bonds are present, resulting in the formation of almost planar P_4 trigonal-pyramidal units. Ni_5P_4 can be better described as a dense packing of the $Ni@P_4$ (blue) distorted tetrahedra and $Ni@P_5$ square pyramids (red) (Figure 1, right).

To investigate the role of Al doping in modification of crystal structure of the phosphides, we investigated the possible structural changes between pure nickel phosphides and their Al-doped analogues. Specifically, we calculated compositions with 8, 25, and 50% of Ni replaced with Al in the Ni_2P crystal structure, and 5, 10, 20, and 50% of Ni replaced with Al in the Ni_5P_4 crystal structure. The resulted ternary Al−Ni−P structures were subjected to structural relaxations. From the comparison of undoped and relaxed most heavily doped analogues, it was established that Al introduction does not lead to significant changes in the crystal structure of the pristine compounds. In particular, different substitutional Al atoms preserve the local coordination of the corresponding Ni atoms in the prototype structures (Figure 2a,b). The only major difference between the structures, for instance, of pure and 50% Al-doped Ni_2P is a small positive chemical pressure created by Al, which is characterized by increased distances to the closest P atom from 2.32 to 2.35 Å as a result of Al and Ni ionic radii differences (Figure 2c,d).

To understand how Al doping changes the electronic structure of the parent compounds, we calculated and compared band structures and density of states (DOS) of

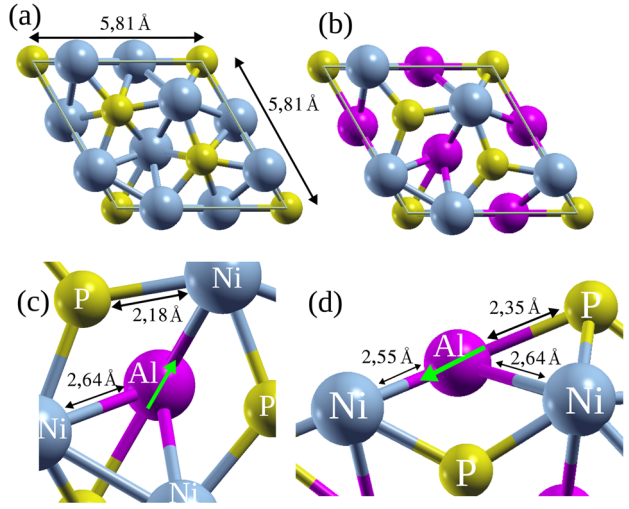

Figure 2. Coordination of the atoms in the crystal structure of pure Ni_2P (a) and its relaxed 50% Al-doped $Al_3Ni_3P_3$ analogues (b−d). Ni: blue; Al: pink; P: yellow.

pure and doped nickel phosphides. The selected band structure plots along the high-symmetry directions of Brillouin zone are shown in Figure S1 in the Supporting Information (SI), whereas the DOS plots together with the orbital projections (PDOS) are represented in Figures S2−S3 (SI). According to the results, both nickel phosphides and their seven calculated doped analogues are metallic in nature without a band gap. The Fermi levels are located in the pseudogap, and the highest contribution to the state below the Fermi level is from Ni(3d) orbitals with some contributions from the P(3p) orbitals, as well as from Al(3p) orbitals for doped systems. Further comparison between total contributions and partial contributions into density of states of Al-doped Ni_2P and Ni_5P_4 clearly demonstrates that increasing Al content leads to a rearrangement of the band structure from localized 3d orbitals into new Al 3p orbitals (Figure 3 and Figure S4, SI). The broadening effect of Al doping on Ni 3d orbitals is stronger in the Ni_2P compound. Moreover, Al doping does not change qualitatively crystal field effects on Ni.

The change in chemical bonding with Al doping is further analyzed by means of electron localization function (ELF). The

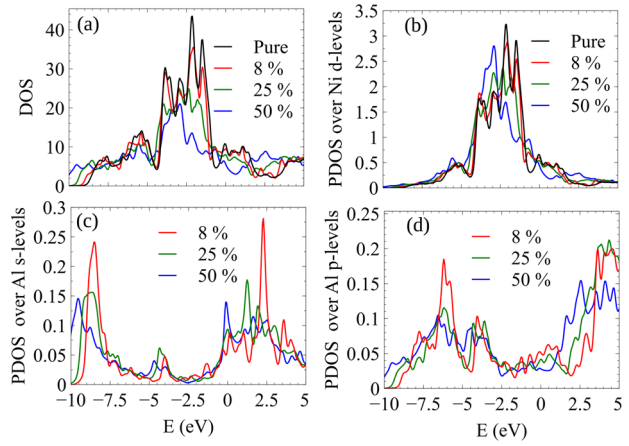

Figure 3. Evolution of density of states in Ni_2P with Al doping: total contribution (a), as well as partial contributions of the Ni 3d orbitals (b), Al 3s orbitals (c) and Al 3p orbitals (d).

DOI: 10.1021/acscatal.5b01761
ACS Catal. 2015, 5, 6503−6508

ELF yields the probability of finding an electron near another electron with the opposite spin, which is typical for chemical bonds and electron lone pairs.[21−24] The ELF for pure and 50% Al-doped Ni_2P and Ni_5P_4 are shown in Figure S5 (SI), projected over the (001) plane. In pristine binary Ni phosphides, there is strong polarization of the Ni−P bonds toward P atoms. The addition of Al in the structure results in the redistribution of the localized electron density and formation of covalent and less polar Al−P bonds.

Using DFT, we examined the preferential location of Al on the Ni phosphide surface. For this, we incorporated Al into the Ni_2P slab in contact with vacuum, as well as into small Ni_2P clusters of 18 atoms. Full structural relaxations of both types of finite fragments were performed. The energy difference between Al atoms on the surface and bulk configuration is 1.7 eV for the cluster and 4.3 eV for the slab. These data show that Al atoms tend to concentrate in the bulk of the system rather than on the surface (Figure S6, SI). Hence, Al should preferentially affect the electronic structure of the produced ternary phases rather than the catalyst surface.

Overall, our DFT results confirm an interesting approach for preparing electrodes with excellent electrocatalytic performance in HER by combining p- and d-metal within the Al−Ni−P system. Specifically, there are several factors suggesting enhanced HER performance of the ternary Al−Ni−P system as a consequence of electronic modification of binary Ni−P: (i) favorable metallic nature of Al−Ni−P, thus ensuring good charge transfer and conductivity of the cathodes; (ii) the development of a broad overall band structure and Ni 3d-subband with doping, which extends over Fermi level; (iii) Al incorporation into Ni phosphides implies that the stability and local electronic structure of the Ni active sites will be affected due to the development of covalent bonding character in presumably ionic Ni−P systems; and (iv) incorporation of Al into Ni phosphides should not perturb significantly the surface and Ni active-site geometry, since Al preferentially resides in the bulk. Therefore, the electrocatalytic activity of Ni phosphides toward HER can be enhanced by Al incorporation as a result of lowering activation energy of hydrogen adsorption on the catalyst surface due to the aforementioned electronic effects.[7,14,25,26]

Because our computations suggested increased HER performance of Al-doped Ni−P electrocatalysts, we moved forward to the synthesis of an Al−Ni−P electrode. Initial experiment involved Al deposition on both sides of the commercially available Ni foam (Figures S7−S9, SI) by sputtering technique (Figures S10−S11, SI). Next, Al-sputtered Ni foam was annealed at 1000 °C for 1 h to provide an Al−Ni alloy foam (Figures S12−S14, SI). Finally, a self-supported Al−Ni−P foam electrode for HER was prepared by gas-transport phosphorization of the Al−Ni sample at 500 °C in phosphorus vapor (Figure S15, SI).[10] A detailed description of the synthesis is presented in the SI.

Powder X-ray diffraction (XRD) revealed that as-synthesized Al−Ni−P electrode is a phase mixture of about 55% of Ni_2P and 45% Ni_5P_4 phases (Figure S16, SI). Although secondary AlP phase could be formed during phosphorization, we ruled out the presence of AlP by XRD analysis, thus indicating that Al-doped Ni_5P_4−Ni_2P electrode material was successfully fabricated (abbreviated as **AlNiP-TT**). The morphology and composition of the Al−Ni−P product were examined by scanning electron microscopy (SEM) in conjunction with energy-dispersive X-ray spectroscopy (EDX). Figure 4 shows

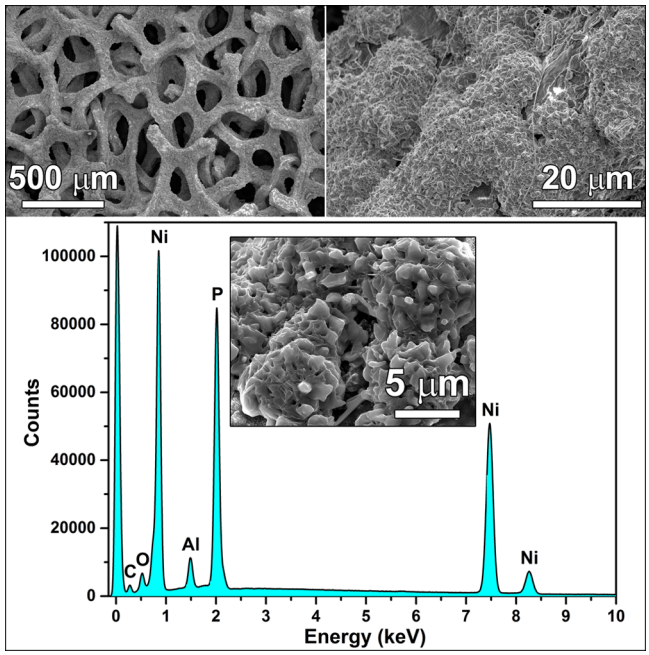

Figure 4. SEM and SEM−EDX studies of self-supported Al−Ni−P foam electrode obtained by gas-transport phosphorization.

that the electrode retained the 3D tangled network morphology of the foam ligaments as compared with bare Ni foam (Figure S8, SI). The surface of the ligaments is covered by large rough aggregates with hard-grained texture. According to SEM−EDX analysis, both surface aggregates and ligaments underneath show the presence of Al, Ni, and P, thus confirming the formation of the desired Al−Ni−P product. Notably, the EDX spectrum shows the presence of O in the sample, although no oxide or phosphate phases were detected by XRD (Figure S16, SI). This suggests that the O signal most likely originates from a slight oxidation of the surface.

Having synthesized the Al−Ni−P electrode, we further evaluated its electrocatalytic activity toward HER in acidic electrolyte. To establish the effect of Al doping on HER performance, we examined the HER activity of two pure Ni−P foam electrodes (abbreviated as **NiP** and **NiP-TT**, Figures S17−18, SI) as controls. We also compared the electrocatalytic activity of our electrodes to that of a commercial Pt/C catalyst with a Pt weight of 20% (abbreviated as 20%Pt/C). More details concerning the reference electrodes and HER testing is presented in the SI.

The results of HER experiments are summarized in Table 1 and Figure 5, showing that the best performance in 0.5 M aqueous H_2SO_4 is expectedly observed for the commercial 20% Pt/C catalyst. Further comparisons among Pt-free electrocatalysts evidence that Al−Ni−P electrode demonstrates the strongest catalytic current on cathodic polarization. Significantly lower currents were recorded for the reference Al-free Ni−P electrodes. For **AlNiP-TT**, an HER onset overpotential, η_{onset} − potential at which the cathodic current density is 1 mA/cm^2 − is only 16 mV, whereas values for pure **NiP** and **NiP-TT** were estimated to be 85 and 81 mV, respectively. Moreover, **AlNiP-TT** reaches cathodic current densities of 10 and 20 mA/cm^2 at overpotentials of ca. 111 mV (η_{10}) and 142 mV (η_{20}), respectively. These values compare favorably to the η_{10} of 175 and 191 mV, as well as with the η_{20} of 225 mV and 251 mV estimated for **NiP** and **NiP-TT**, respectively. In addition, the

DOI: 10.1021/acscatal.5b01761
ACS Catal. 2015, 5, 6503−6508

Table 1. Electrocatalytic Properties of the Self-Supported Phosphides Electrodes

electrode	AlNiP-TT	NiP	NiP-TT	20%Pt/C
mass density (mg/cm^2)	54.1	59.4	56.9	0.283
η_{onset}, onset potential for driving 1 mA/cm^2 (mV)	16	85	81	6.4
η_{10}, current densities of 10 mA/cm^2 (mV)	111	175	191	24
η_{20}, current densities of 20 mA/cm^2 (mV)	142	225	251	36
j_0, exchange current density (mA/cm^2)[a]	0.60	0.21	0.26	6.40
Tafel slope (mV/dec)[a]	75.3	126.3	165.0	36.3
Tafel slope (mV/dec)[b]	65	84	90	33
C_{dl}, double-layer capacitance (mF/cm^2)[c]	20.4	19.7	14.7	–

[a]Estimated using EC-Lab software (Bio-Logic) without *iR* compensation (Figures S19–21, SI). [b]Estimated using *iR* compensation (Figure S22). [c]Estimated by linear fitting of the data representing anodic and cathodic difference in current density as a function of cyclic voltammetry scan rate (Figure S24, SI).[27]

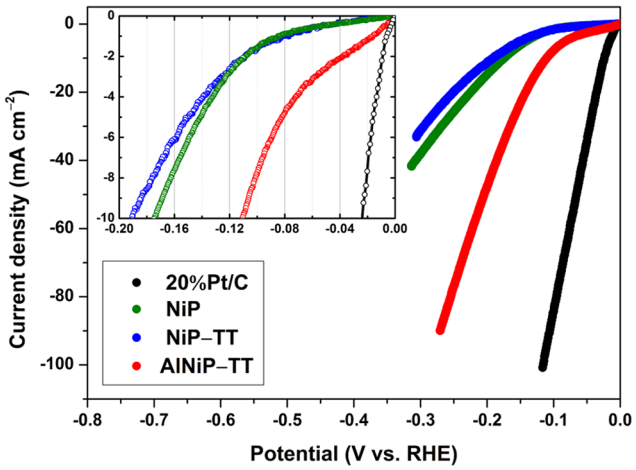

Figure 5. Cathodic polarization curves of the synthesized and reference electrodes, which were scanned anodically at 2 mV/s (10 mV/s for 20%Pt/C). All polarization curves are *iR*-compensated.

prepared Al–Ni–P electrocatalyst also shows a remarkably high exchange current density, j_0, and a reasonably small Tafel slope. In particular, analysis of the electrocatalytic data shows that **AlNiP-TT** roughly doubly outperforms reference Ni–P electrocatalysts, offering j_0 of 0.6 mA/cm^2 and a Tafel slope of ca. 65 mV/decade (Table 1 and Figures S19–22, SI). Importantly, the latter slope value is in the 38–116 mV/decade range, suggesting a Volmer–Heyrovsky mechanistic scenario, wherein the rate of the discharge step is comparable with the desorption step during the HER process.[28−31]

We also characterized the **AlNiP-TT** electrode by electrochemical impedance spectroscopy (EIS), and the parameters obtained by fitting the Nyquist plots to the equivalent circuit model are summarized in Figure S23 and Table S1 (SI). At zero potential versus RHE, the equivalent series resistance, R_s, electron/charge transport resistance, R_1, and charge transfer resistance, R_{ct}, were estimated to be only 0.78, 1.35, and 8.46 Ω, respectively. These values indicate small internal resistance of the electrode, as well as suggest fast charge-transfer kinetics over **AlNiP-TT**/electrolyte interface.[9,10,28]

Notably, the observed high performance of Al-containing **AlNiP-TT** in comparison with that of pure nickel phosphide **NiP** and **NiP-TT** reference electrodes does not correlate with the phase composition. Specifically, both **NiP** and **NiP-TT** were found to contain Ni_5P_4 as the major phase (Figures S17–18, SI), which is reported to have higher activity for HER and better stability in acidic solutions than the Ni_2P phase.[32,33] Furthermore, we estimated the double-layer capacitance, C_{dl}, of **NiP**, **NiP-TT**, and **AlNiP-TT** electrodes (Table 1, Figure S24) to evaluate the effective electrochemically active surface area of the solid–liquid interface.[27] Comparison of C_{dl} values reveals that there is no significant increase in relative effective surface area with Al doping. The facts that **AlNiP-TT** has Ni_2P as the abundant phase (Figure S16, SI) and electrochemically active surface area similar to those of the reference electrodes (Figure S24, SI) while exhibiting remarkable high performance (Figure 5) suggest that the presence of Al conceivably increases electrode activity, as theoretically predicted.

The stability and durability of the developed Al–Ni–P electrocatalyst were also studied on sample **AlNiP-TT** by means of accelerated degradation test (ADT) and chronopotentiometry. Figure S25 compares the initial cathodic polarization curve to the one after 1000 cycles. Upon cycling in a range of −300–60 mV vs RHE at a rate of 50 mV/s, the activity of the electrode decreases ca. 25%. After ADT, the durability of the Al–Ni–P electrode was evaluated at a fixed overpotential of 100 mV. The cathodic current density was found to slightly decrease from 3 to 2.5 mA/cm^2 during the initial 5 h of testing and thereafter stabilize at the latter value, which is remarkably higher than that of metallic Ni foam or Pt foil electrodes.[9]

We associate the aforementioned loss of activity with the corrosion of the **AlNiP-TT** sample via partial dissolution, which was confirmed by XRD and SEM studies of the electrode composition and morphology before and after stability and durability tests (Figure S26–S27, SI). Because Al can be easily dissolved by acids, one could expect that the observed corrosion of the Al–Ni–P electrode results from Al leaching. EDX analysis, however, reveals the presence of Al in the tested electrode, suggesting partial dissolution of the whole Al–Ni–P electrode and not Al exclusively (Figure S27, SI). This is further confirmed by inductively coupled plasma–optical emission spectroscopy (ICP–OES) analysis of electrolyte samples, which were collected after ADT for 1000 cycles and durability testing for 24 h, as well as after subsequent durability testing for additional 24 h. According to the ICP–OES, both Al and Ni leach to the electrolyte solution during testing, thus supporting the hypothesis of overall Al–Ni–P electrode corrosion (Table S2, SI). Nevertheless, the stability and durability of the highly active Al–Ni–P electrode for HER might be further improved by optimizing the Al to Ni ratio and phase composition of the electrode and microstructure; these are the subject of our current experimental efforts.

In summary, in our efforts to replace Pt in HER, we proposed a new class of highly active electrocatalysts based on the combination of p- and d-metal in a phosphide compound, and we used DFT calculations to investigate the structural and electronic modifications of nickel phosphides by Al doping as a model but previously unreported system. DFT computations suggest development of a broad band structure and covalent-bonding character with Al doping, which is presumed to result in an Al–Ni–P electrode having enhanced electrocatalytic activity as compared to pure nickel phosphide. Most

DOI: 10.1021/acscatal.5b01761
ACS Catal. 2015, 5, 6503–6508

importantly, our experimental results fully supported the DFT predictions, offering an Al−Ni−P electrode exhibiting activity superior to that of pure Ni−P, as well as reported Ni−P and state-of-the-art MoS_2/RGO, Mo_2C/CNT, mesoporous Mo_2C, 1T−WS_2, mixed metal $(Fe_{0.48}Co_{0.52})S_2$, and other transition-metal phosphide electrocatalysts (Figure 6).[8−10,31,32,34−43] Only

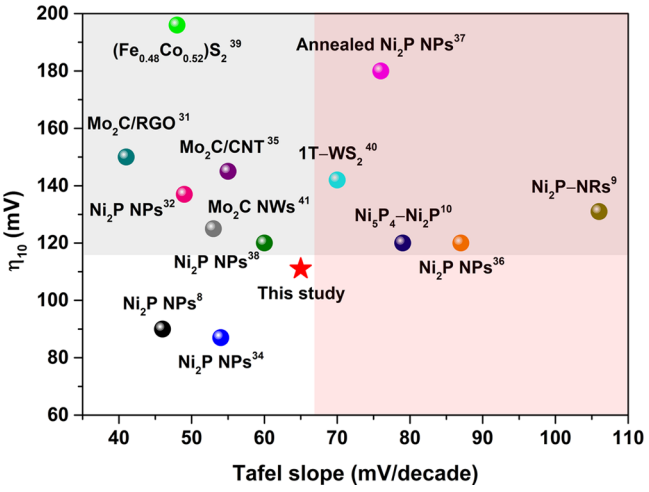

Figure 6. Tafel slope and η_{10} comparison of our Al−Ni−P electrocatalyst with the state-of-the-art HER electrocatalysts based on earth-abundant elements.

two nickel phosphides in nanoparticulate form have higher activity than our Al−Ni−P cathode, most likely because of their high surface areas typical for nanoparticles. Overall, the unique approach proposed herein can be extended to obtain various electrocatalysts for water splitting based on p- and d-metal-containing pnictides.

■ ASSOCIATED CONTENT

Supporting Information

The Supporting Information is available free of charge on the ACS Publications website at DOI: 10.1021/acscatal.5b01761.

Materials and methods and additional DFT, synthesis, XRD, SEM, EDX, and electrocatalytic data (PDF)

■ AUTHOR INFORMATION

Corresponding Author

*E-mail: yury.kolenko@inl.int.

Notes

The authors declare no competing financial interest.

■ ACKNOWLEDGMENTS

We thank all members of the Nanomaterial Synthesis Laboratory at the INL, and especially Dr. L. M. Salonen, for valuable discussions and critical comments. This work was supported by European Regional Development Fund within ON.2 − O Novo Norte Program. J.L.L. acknowledges the Marie-Curie-ITN607904-SPINOGRAPH project for a Ph.D. grant, whereas X.G.W. thanks the Marie-Curie-COFUND-NanoTrainforGrowth programme for a postdoctoral grant. C.R.-A. is grateful to EU FP7 Cooperation Program for funding through NMP-theme (grant no. 314212). L.-F.L. acknowledges the FCT Investigator Grant (no. IF/01595/2014) for support.

■ REFERENCES

(1) Parsons, R. *Trans. Faraday Soc.* **1958**, *54*, 1053−1063.
(2) Kibria, M. F.; Mridha, M. S.; Khan, A. H. *Int. J. Hydrogen Energy* **1995**, *20*, 435−440.
(3) Morales-Guio, C. G.; Stern, L. A.; Hu, X. L. *Chem. Soc. Rev.* **2014**, *43*, 6555−6569.
(4) Markovic, N. M.; Grgur, B. N.; Ross, P. N. *J. Phys. Chem. B* **1997**, *101*, 5405−5413.
(5) Vesborg, P. C. K.; Seger, B.; Chorkendorff, I. *J. Phys. Chem. Lett.* **2015**, *6*, 951−957.
(6) Bodner, M.; Hofer, A.; Hacker, V. *WIREs Energy Environ.* **2015**, *4*, 365.
(7) Liu, P.; Rodriguez, J. A. *J. Am. Chem. Soc.* **2005**, *127*, 14871−14878.
(8) Popczun, E. J.; McKone, J. R.; Read, C. G.; Biacchi, A. J.; Wiltrout, A. M.; Lewis, N. S.; Schaak, R. E. *J. Am. Chem. Soc.* **2013**, *135*, 9267−9270.
(9) Wang, X. G.; Kolen'ko, Y. V.; Liu, L. F. *Chem. Commun.* **2015**, *51*, 6738−6741.
(10) Wang, X.; Kolen'ko, Y. V.; Bao, X.-Q.; Kovnir, K.; Liu, L. *Angew. Chem. Int. Ed.* **2015**, *127*, 8306−8310.
(11) Studt, F.; Abild-Pedersen, F.; Bligaard, T.; Sorensen, R. Z.; Christensen, C. H.; Norskov, J. K. *Science* **2008**, *320*, 1320−1322.
(12) Armbruster, M.; Kovnir, K.; Friedrich, M.; Teschner, D.; Wowsnick, G.; Hahne, M.; Gille, P.; Szentmiklosi, L.; Feuerbacher, M.; Heggen, M.; Girgsdies, F.; Rosenthal, D.; Schlogl, R.; Grin, Y. *Nat. Mater.* **2012**, *11*, 690−693.
(13) Kovnir, K.; Armbruster, M.; Teschner, D.; Venkov, T. V.; Jentoft, F. C.; Knop-Gericke, A.; Grin, Y.; Schlogl, R. *Sci. Technol. Adv. Mater.* **2007**, *8*, 420−427.
(14) Hammer, B.; Norskov, J. K. *Adv. Catal.* **2000**, *45*, 71−129.
(15) Schlogl, R. *Angew. Chem. Int. Ed.* **2015**, *54*, 3465−3520.
(16) Dong, H. X.; Lei, T.; He, Y. H.; Xu, N. P.; Huang, B. Y.; Liu, C. T. *Int. J. Hydrogen Energy* **2011**, *36*, 12112−12120.
(17) Erlebacher, J.; Aziz, M. J.; Karma, A.; Dimitrov, N.; Sieradzki, K. *Nature* **2001**, *410*, 450−453.
(18) Greeley, J.; Jaramillo, T. F.; Bonde, J.; Chorkendorff, I. B.; Norskov, J. K. *Nat. Mater.* **2006**, *5*, 909−913.
(19) Giannozzi, P.; Baroni, S.; Bonini, N.; Calandra, M.; Car, R.; Cavazzoni, C.; Ceresoli, D.; Chiarotti, G. L.; Cococcioni, M.; Dabo, I.; Dal Corso, A.; de Gironcoli, S.; Fabris, S.; Fratesi, G.; Gebauer, R.; Gerstmann, U.; Gougoussis, C.; Kokalj, A.; Lazzeri, M.; Martin-Samos, L.; Marzari, N.; Mauri, F.; Mazzarello, R.; Paolini, S.; Pasquarello, A.; Paulatto, L.; Sbraccia, C.; Scandolo, S.; Sclauzero, G.; Seitsonen, A. P.; Smogunov, A.; Umari, P.; Wentzcovitch, R. M. *J. Phys.: Condens. Matter* **2009**, *21*, 395502.
(20) The Elk FP-LAPW Code. http://elk.sourceforge.net/.
(21) Becke, A. D.; Edgecombe, K. E. *J. Chem. Phys.* **1990**, *92*, 5397−5403.
(22) Grin, Y.; Savin, A.; Silvi, B. The ELF Perspective of chemical bonding. In *The Chemical Bond: Fundamental Aspects of Chemical Bonding*; Frenking, G., Shaik, S., Eds.; Wiley-VCH Verlag GmbH & Co. KGaA: Weinheim, 2014; pp 345−382.
(23) Savin, A.; Jepsen, O.; Flad, J.; Andersen, O. K.; Preuss, H.; Vonschnering, H. G. *Angew. Chem., Int. Ed. Engl.* **1992**, *31*, 187−188.
(24) Savin, A.; Nesper, R.; Wengert, S.; Fassler, T. F. *Angew. Chem. Int. Ed.* **1997**, *36*, 1808−1832.
(25) Quaino, P.; Santos, E.; Soldano, G.; Schmickler, W. *Adv. Phys. Chem.* **2011**, *2011*, 851640.
(26) Moon, J.-S.; Jang, J.-H.; Kim, E.-G.; Chung, Y.-H.; Yoo, S. J.; Lee, Y.-K. *J. Catal.* **2015**, *326*, 92−99.
(27) Faber, M. S.; Dziedzic, R.; Lukowski, M. A.; Kaiser, N. S.; Ding, Q.; Jin, S. *J. Am. Chem. Soc.* **2014**, *136*, 10053−10061.
(28) Huang, Z. P.; Chen, Z. Z.; Chen, Z. B.; Lv, C. C.; Humphrey, M. G.; Zhang, C. *Nano Energy* **2014**, *9*, 373−382.
(29) Gao, M. R.; Lin, Z. Y.; Zhuang, T. T.; Jiang, J.; Xu, Y. F.; Zheng, Y. R.; Yu, S. H. *J. Mater. Chem.* **2012**, *22*, 13662−13668.

DOI: 10.1021/acscatal.5b01761
ACS Catal. 2015, 5, 6503−6508

(30) Chen, W. F.; Iyer, S.; Iyer, S.; Sasaki, K.; Wang, C. H.; Zhu, Y. M.; Muckerman, J. T.; Fujita, E. *Energy Environ. Sci.* **2013**, *6*, 1818−1826.
(31) Li, Y. G.; Wang, H. L.; Xie, L. M.; Liang, Y. Y.; Hong, G. S.; Dai, H. J. *J. Am. Chem. Soc.* **2011**, *133*, 7296−7299.
(32) Pan, Y.; Liu, Y. R.; Zhao, J. C.; Yang, K.; Liang, J. L.; Liu, D. D.; Hu, W. H.; Liu, D. P.; Liu, Y. Q.; Liu, C. G. *J. Mater. Chem. A* **2015**, *3*, 1656−1665.
(33) Kucernak, A. R. J.; Sundaram, V. N. N. *J. Mater. Chem. A* **2014**, *2*, 17435−17445.
(34) Bai, Y. J.; Zhang, H. J.; Li, X.; Liu, L.; Xu, H. T.; Qiu, H. J.; Wang, Y. *Nanoscale* **2015**, *7*, 1446−1453.
(35) Chen, W. F.; Wang, C. H.; Sasaki, K.; Marinkovic, N.; Xu, W.; Muckerman, J. T.; Zhu, Y.; Adzic, R. R. *Energy Environ. Sci.* **2013**, *6*, 943−951.
(36) Feng, L. G.; Vrubel, H.; Bensimon, M.; Hu, X. L. *Phys. Chem. Chem. Phys.* **2014**, *16*, 5917−5921.
(37) Lu, A. L.; Chen, Y. Z.; Li, H. Y.; Dowd, A.; Cortie, M. B.; Xie, Q. S.; Guo, H. Z.; Qi, Q. Q.; Peng, D. L. *Int. J. Hydrogen Energy* **2014**, *39*, 18919−18928.
(38) Pu, Z. H.; Liu, Q.; Tang, C.; Asiri, A. M.; Sun, X. P. *Nanoscale* **2014**, *6*, 11031−11034.
(39) Faber, M. S.; Lukowski, M. A.; Ding, Q.; Kaiser, N. S.; Jin, S. *J. Phys. Chem. C* **2014**, *118*, 21347−21356.
(40) Lukowski, M. A.; Daniel, A. S.; English, C. R.; Meng, F.; Forticaux, A.; Hamers, R. J.; Jin, S. *Energy Environ. Sci.* **2014**, *7*, 2608−2613.
(41) Liao, L.; Wang, S. N.; Xiao, J. J.; Bian, X. J.; Zhang, Y. H.; Scanlon, M. D.; Hu, X. L.; Tang, Y.; Liu, B. H.; Girault, H. H. *Energy Environ. Sci.* **2014**, *7*, 387−392.
(42) Zeng, M.; Li, Y. G. *J. Mater. Chem. A* **2015**, *3*, 14942−14962.
(43) Faber, M. S.; Jin, S. *Energy Environ. Sci.* **2014**, *7*, 3519−3542.

DOI: 10.1021/acscatal.5b01761
ACS Catal. 2015, 5, 6503−6508